RSC Advances

PAPER

View Article Online
View Journal | View Issue

Cite this: *RSC Adv.*, 2024, **14**, 31624

Na^+ detection *via* brightening of synergistically originated noble metal nanoclusters†

Priyanka Sharma, Mainak Ganguly * and Mamta Sahu

Received 29th July 2024
Accepted 30th September 2024

DOI: 10.1039/d4ra05501b

rsc.li/rsc-advances

Weakly fluorescent AuAg nanoclusters were obtained from glutathione, chloroauric acid, and silver nitrate aqueous solution under a modified hydrothermal method. Such glutathione-capped synergistically evolved clusters were obtained for the first time by employing our experimental conditions. Such weak fluorescence was made significantly brighter by employing Na^+ and a Na^+ sensor was obtained with a linear detection range of 10^{-5}–5×10^{-9} M, while the limit of detection was 1.02×10^{-6} M. Na^+ made the GSH matrix positively charged to stabilize AuAg clusters resulting in strong emissive properties. Furthermore, the effect of solvents, sunlight exposure, and temperature was gauged. Estimation of Na^+ concentration was undertaken for natural water samples to demonstrate the practical utility of the designed nanosensor.

1. Introduction

In the body, sodium is an essential alkali metal that plays a key role in extracellular fluid.[1] It is responsible for regulating the water level and electrolyte balance. It is a naturally occurring blood serum component with a normal range of 135–145 mM.[2] It is responsible for preserving the blood ionic equilibrium; yet any variation in its concentration raises the risk of hypertension, diabetes, heart failure, stroke, and renal issues. It is possible to use the quantity of sodium found in water resources as a direct indicator of salinity, and it may be possible to avoid excessive salinization by regularly checking the concentration of sodium in water bodies.[3] Because of its intimate connection to human health, researchers have been working hard to develop sodium-ion sensors that are economical, sensitive, and discriminating.[4]

Over the past few decades, metal nanostructures—particularly metal nanoparticles and nanoclusters—have been the topic of extensive research and development in nanotechnology because of their unique optical, magnetic, and catalytic characteristics.[5] Nanoclusters, a type of nanoparticle, bridge the gap between atoms and nanocrystals and make important contributions to basic and applied study. Their molecule-like qualities, like quantized charging and luminosity, are more likely to be used to make new products. Fluorescent metal nanoclusters have been widely employed as sensors because of their ability to respond to changes in their medium such as temperature, oxidative stress, acidity, and the presence of various chemicals such as metal ions.[6] Due to their low stability, only a few methods for synthesizing fluorescent silver nanoclusters have been described, even though gold nanoclusters have been thoroughly studied over the past ten years. The Ag nanocluster exhibits more strong fluorescence than the Au nanocluster, which increases its usefulness for several important applications.[7,8] Thiolate often synthesizes and protects gold and silver nanoclusters. Synergistic impact occurs when two or more species have a stronger influence than their separate effects. Gold–silver synergism for nanocluster formation is an active area of research due to autofluorescence, doping/alloying, aggregation-induced fluorescence, oxidation and interaction-induced fluorescence enhancement, and silver effect.[8]

In this paper, we reported a Na^+ sensor employing the fluorescence enhancement of weakly fluorescence AuAg nanoclusters. For the fluorescence enhancement intensification of the positive charge of the matrix was the pivotal factor (Scheme 1).

2. Results and discussion

2.1 Synergistically evolution of weakly fluorescent AuAg nanoclusters

A decent fluorescent AuAg cluster was obtained by mixing silver nitrate, chloroauric acid, and glutathione (GSH) with 6 h aging under a 100 W bulb. The pale yellow-colored AuAg nanoclusters exhibited fluorescence (λ_{ex} 290 nm and λ_{em} 405 nm). Notably, silver and gold were inevitably to originate AuAg fluorescent clusters. Only chloroauric acid with GSH or silver nitrate with GSH could not generate fluorescent species after hydrothermal treatment. Thus, synergism between gold and silver was mandatory for the evolution of fluorescence species. There was no signature of the surface plasmon[10] band of gold nanoparticles and silver nanoparticles in AuAg@GSH hydrosol, indicating the formation of nanoclusters. Nanoclusters, the

Solar Energy Conversion and Nanomaterials Laboratory, Department of Chemistry, Manipal University Jaipur, Dehmi Kalan, Jaipur 303007, India. E-mail: mainak.ganguly@jaipur.manipal.edu

† Electronic supplementary information (ESI) available: UV, XPS, IR, DLS, LCMS, bar diagram, fluorescence spectra. See DOI: https://doi.org/10.1039/d4ra05501b

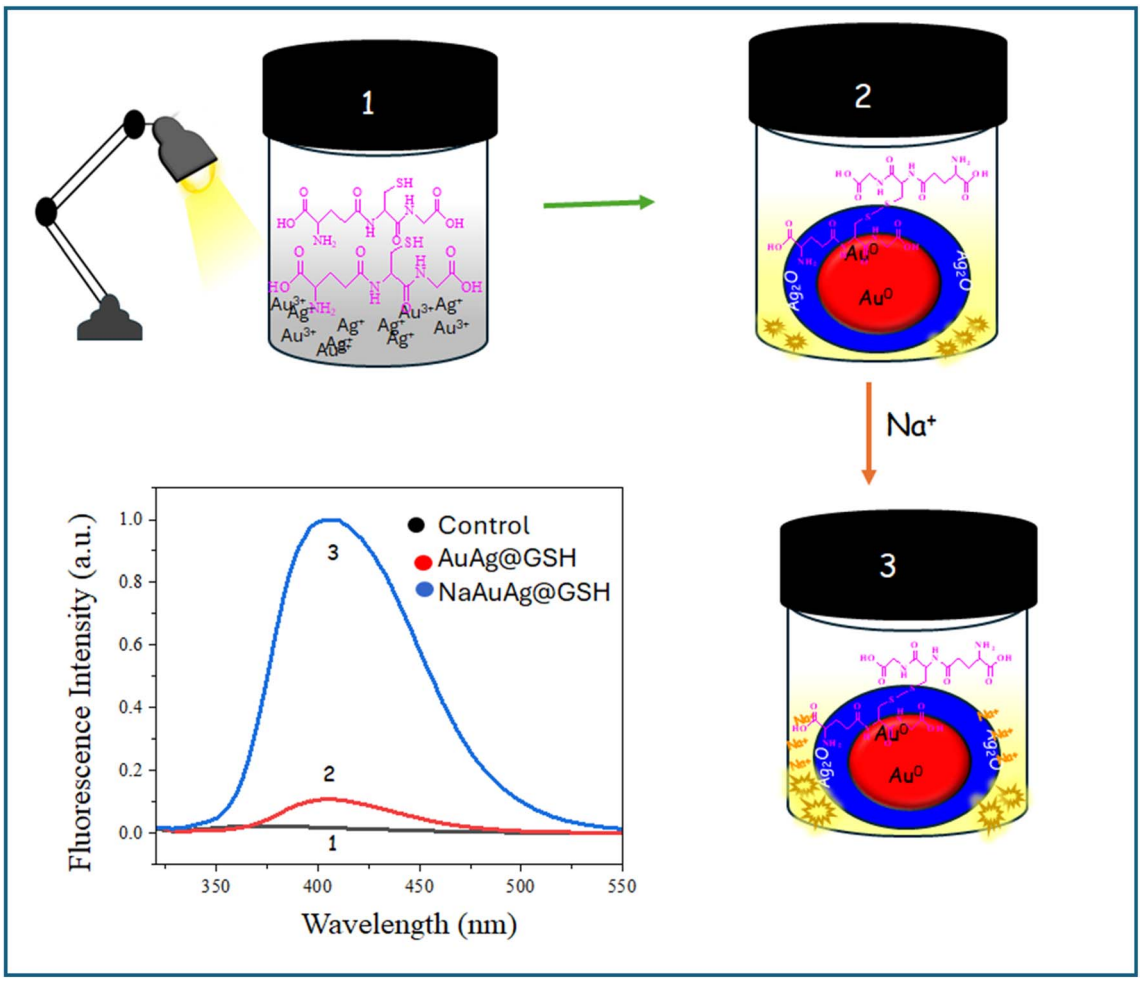

Scheme 1 Na^+ highly enhanced the fluorescence of hydrothermally synthesized AuAg@GSH.

missing link between nanoparticles and atoms, have ultra-small size (<2 nm) with few atoms and discrete energy levels. The number of atoms in nanoclusters is insufficient to originate the surface plasmon band.[11] The absorption peak at λ_{max} 356 nm and 277 nm of Ag@GSH hydrosol was remarkably suppressed in AuAg@GSH hydrosol indicating the formation of AuAg core–shell particles [Fig. S1, ESI†]. Though some reports of GSH passivated AuAg nanoclusters are found in literature, nanoclusters with λ_{ex} 290 nm and λ_{em} 405 nm are disclosed here for the first time (Table 1).

The pale-yellow color AuAg@GSH hydrosol contained spherical particles as evident from the FESEM image. EDAX spectra showed that the atomic percent of silver was five times higher than that of gold, although we added chloroauric acid and silver nitrate to equal molar concentration. Such observation indicated that silver was as a shell, and gold was as a core. Gold forms the core and silver form the shell in core–shell particles because gold has a lower reduction potential, leading it to nucleate first, while silver, with a higher reduction potential, deposits later around the gold core.[11] So, the fluorescent

Table 1 GSH passivated AuAg nanoclusters with properties and applications

Precursors	$\lambda_{ex}/\lambda_{em}$	Size/shape	Experimental condition	Application
Glutathione S transferase (Cao *et al.* 2022)[9]	395 nm/477 nm or 653 nm	—	—	Oxytetracycline sensing
GSH (Zhang *et al.* 2015)[9]	380 nm/618 nm	3.2 nm(DLS)/spherical	Heat in microwave at 90 °C	Anion sensing
GSH (Liu *et al.* 2018)[9]	360 nm/616 nm & 512 nm	1 nm/dispersed shape	Incubated 80 °C in 6 h	Cysteine sensing
GSH (Ganguly *et al.* 2013)[9]	400/564 nm	Spherical	Under sunlight ~12 h	Antibacterial activity
GSH (Ganguly *et al.* 2014)[11]	400 nm/564 nm	600 nm/spherical	Under the sun ~3 h	Hg^{2+} sensing
GSH (this work)	290 nm/405 nm	265 nm(DLS)/spherical	Under bulb ~6 h	Na^+ sensing

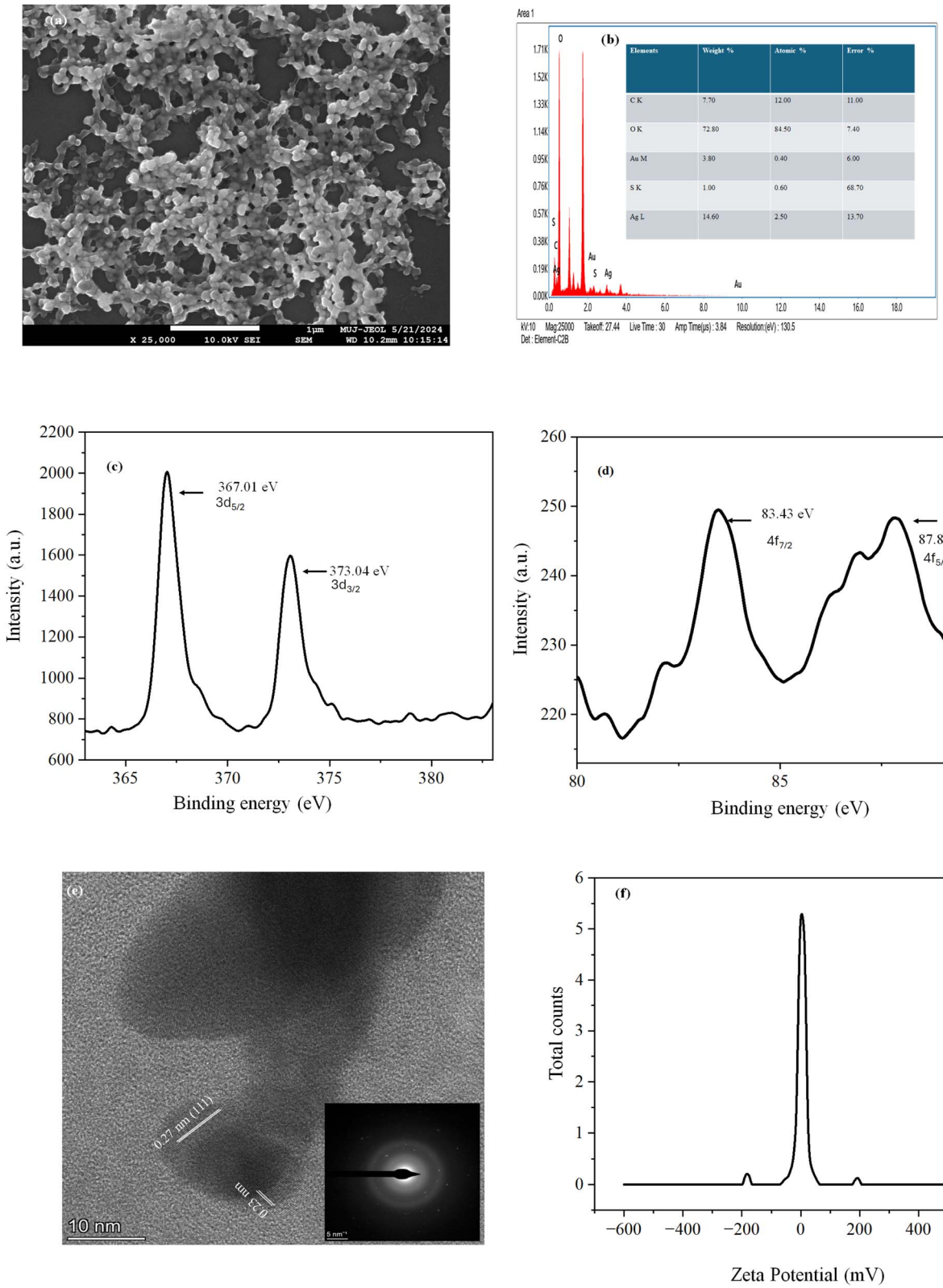

Fig. 1 (a) FESEM, (b) EDAX (c) XPS of Ag_2O, (d) XPS of Au^0, (e) TEM & SAED and (f) zeta potential of AuAg@GSH.

species was Ag_{shell}–Au_{core}@GSH. TEM image also confirmed the core–shell nature. HRTEM image implied a lattice fringe of 0.27 nm for the Ag_2O shell and 0.23 nm for the Au (0) core. SAED image indicated poly crystallinity.[12] Binding energies of Au 83.43 eV and 87.87 eV corroborated with Au $4f_{7/2}$ and Au $4f_{5/2}$ respectively, when Au was in zero oxidation state. Binding

energies of Ag 373.04 eV and 367.01 eV corroborated with Ag $3d_{3/2}$ and Ag $3d_{5/2}$ respectively, when Ag is in Ag_2O state. The solution was stable with a negative zeta potential (−0.26 mV)[13] [Fig. 1]. A high level of stability in a colloidal system can be attributed to a variety of variables, even though a low zeta potential is often indicative of a greater possibility of aggregation. The stability of the nanocluster was mostly due to the presence of steric stabilization, depletion flocculation (which included selective adhesion, specific interaction, and kinetic interaction), and delayed aggregation.[14] The XPS spectra contained S $2p_{3/2}$ and S $2p_{1/2}$ components at 162.4 eV and 163.6 eV, respectively, which agreed with the typical values for chemisorbed thiolated forms and a very weak peak that can be fitted into one signals at 163.6 eV corresponding to C–S.[15] Two minor peaks at higher energy (166.0 eV and 167.3 eV) were consistent with the –C–S(O)$_2$–C– sulfone bridge [Fig. S2, ESI†]. Solution phase IR spectrum of AuAg@GSH indicated a strong Ag–S peak at 524 cm^{-1}, unlike GSH solution.[16,17] DLS analysis indicated an average hydrodynamic diameter of 265 nm [Fig. S3, ESI†]. Particle size distribution was tight with 93% particles at ~261 nm. As tiny AuAg clusters were anchored on the GSH matrix DLS got greater hydrodynamic diameter. The hydrodynamic diameter is typically larger than the size observed in electron microscopy due to the inclusion of the solvation shell or hydration layer surrounding particles in solution, which contributes to the overall measured size in hydrodynamic techniques like dynamic light scattering (DLS).[13] Electron microscopy, in contrast, measures the core size of particles without accounting for the solvent layer. LCMS revealed the cluster formation responsible for the origin of fluorescence. We

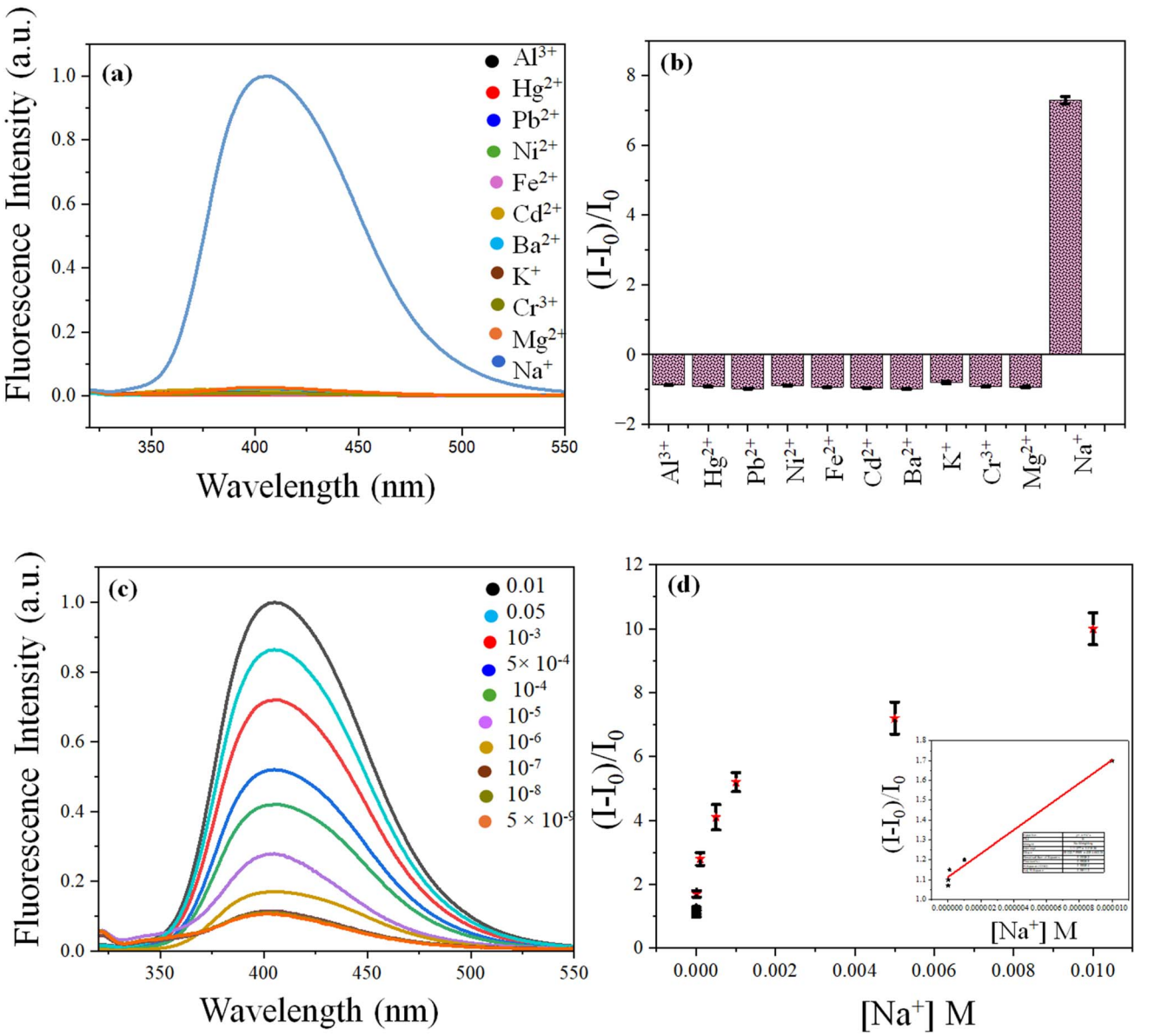

Fig. 2 (a) Fluorescence spectra and (b) bar diagram of AuAg@GSH with metal ion; (c) fluorescence spectra of AuAg@GSH with [Na^+] and (d) LOD estimation of Na^+ detection.

obtained (Ag_2Au_2 + 2S), (GSH + AuAgO + Cl), (Ag_2Au_2 + 2S), (Au_2 + GSH) fragments [Fig. S4, ESI†].

As per the literature, diverse mechanisms regarding AuAg synergism for the evolution of strong fluorescence are available. Wu *et al.*[18] reported that silver ions were required to obtain higher emissions after the completion of $Au_{25}(SG)_{18}$ due to certain structured complexes. Added Ag^+ resulted in the chelation-enhanced fluorescence (CHEF) mechanism for the increment of fluorescence of $Au_{25}(SG)_{18}$. Zhang *et al.*[19] also revealed the speedy synthesis of GSH-capped AuAg NCs (GSAuAg NCs) *via* microwave irradiation. Ag/Au 0.2 brought maximum quantum yield. Charge redistribution of Au–Ag to compensate for the electron-withdrawing properties of the thiolate was attributed to the cluster stability. The Au–Ag charge redistribution, that occurred within the clusters, balanced the electron-withdrawing effects of the thiolate ligand. CHEF and charge redistribution were attributed to be the pivotal factors for the synergistic evolution of fluorescence.

2.2 Selective and sensitive Na^+ stimulated fluorescence enhancement: a sensing platform

Sodium ion exclusively and instantaneously enhanced the fluorescence of AuAg@GSH to a large extent, forming NaAuAg@GSH. No other metal ions (Al^{3+}, Hg^{2+}, Pb^{2+}, Ni^{2+}, Fe^{2+}, Cd^{2+}, Ba^{2+}, K^+, Cr^{3+}, Mg^{2+}, Na^+) could enhance the fluorescence indicating that AuAg was a highly selective sensing platform for a Na^+ sensing. The detection limit was 1.02×10^{-6} M and ranges from 10^{-5} M to 5×10^{-9} M (R^2 0.985) [Fig. 2].

The interfering metal ions did not alter the enhanced fluorescence of NaAuAg@GSH significantly (Fig. S5, ESI†). As observed in Fig. S5,† Cu^{2+} decreased the fluorescence of NaAuAg@GSH. Like Au and Ag, Cu^{2+} is also group 11 element in the periodic table with the smallest size and high penetrating power. Copper could make a strong complex with GSH, destroying the capping of AuAg clusters.[20] Thus, the highest quenching was observed for Cu^{2+}. For Pb^{2+}, Co^{3+}, and Cr^{3+} metal ions, quenching was observed due to their influence on the capping agent (GSH-GSSG) at various extents. Little enhancement was observed for Ba^{2+}, Hg^{2+}, and Al^{3+} metal ions due to the further stability of NaAuAg@GSH clusters.

2.3 Natural water sample analysis

We collected water samples from various locations, including the Ganga River in Haridwar, drinking water in Jaipur, rainwater in Jaipur, and tap water in Jaipur itself. Several different concentrations of Na^+ were added to the water. The fluorometric sensing techniques, discussed in the study, were utilized by us to determine the presence of Na^+ in the water. Table 2, shows that the findings that were obtained were quite close to the amounts that were spiked.

2.4 Effect of various solvents on fluorescence enhancement

The exclusive fluorescence enhancement stimulated by fluorescence was observed in an aqueous system and water-miscible organic solvents. Table 3 indicates the various enhancements with the different solvents. An increase in dielectric constant was associated with increased Na^+ stimulated fluorescence enhancement indicating that polarity stabilized the NaAuAg@GSH clusters. This trend was interrupted for DMSO (low dielectric constant/high enhancement) and acetone (high dielectric constant/low enhancement).

For the case of the DMSO (dielectric constant 1), enhancement was higher than other solvents with higher dielectric constants. DMSO is a sulfur-containing solvent with the –S═O bond.[21] DMSO further enhanced the protection of GSH/GSSG and enhanced the stability of NaAuAg@GSH. Noble metal–sulfur interaction was the driving force behind the stability and enhanced fluorescence behavior of NaAuAg@GSH in DMSO with low dielectric constant.

2.5 Influence of temperature on fluorescence enhancement

For novel metal nanoclusters, photostability and thermal stability are a challenge. We investigated the effect of temperature (25–65 °C) on AuAg@GSH and NaAuAg@GSH. For both cases, fluorescence decreased with an increase in temperature, starting from room temperature (25 °C). Enhanced Brownian motion[22] with increased temperature was pivotal for such a decrement. However, in the absence of NaAuAg@GSH, the decrease in fluorescence was quite rapid for AuAg@GSH up to 60 °C. Thus, the Na^+ matrix contributed extra thermal stability

Table 2 Determination of Na^+ from natural water

Sample name	Added [Na^+] (M)	[Na^+] detected (M)	Recovery (%)	Relative error (%)	RSD (%) ($n = 3$)
Rainwater (Jaipur)	5.00×10^{-5}	4.91×10^{-5}	98.2	1.8	1.5
	5.00×10^{-4}	4.01×10^{-4}	80.2	19.8	0.9
	5.00×10^{-3}	4.02×10^{-3}	80.4	19.6	0.7
Drinking water (Jaipur)	5.00×10^{-5}	4.89×10^{-5}	97.8	2.5	1.3
	6.00×10^{-4}	5.89×10^{-4}	98.1	1.9	0.9
	5.00×10^{-3}	5.04×10^{-3}	100.8	0.8	0.5
Tap water (Jaipur)	7.00×10^{-5}	7.10×10^{-5}	101.4	1	1.8
	7.00×10^{-4}	6.05×10^{-4}	86.4	14	1.1
	7.00×10^{-3}	7.88×10^{-3}	112.5	2	0.3
Ganga river (Haridwar)	5.00×10^{-5}	4.87×10^{-5}	97.4	3	1.8
	5.00×10^{-4}	4.11×10^{-4}	82.2	17.8	1.6
	5.00×10^{-3}	6.98×10^{-3}	139.6	39	0

Table 3 Na^+ induced enhancements of AuAg@GSH in various solvents

Solvents	Extent of enhancement	Dielectric constant
Chloroform	0.76	1.4
Tetrahydrofuran	0.29	7.58
DMSO (dimethyl sulfoxide)	4.29	1.0
Ethanol	3.34	24.3
Methanol	4.00	32.7
Acetone	0.89	20.7
IPA (isopropyl alcohol)	2.24	19.92
Ethyl acetate	0.73	6.02
DCM (dichloromethane)	0.79	8.93
H_2O	10.36	80.1

towards AuAg@GSH clusters. I_T/I_{RT} (I_{RT} = fluorescence intensity at room temperature; I_T = fluorescence intensity at temperature T) *vs.* temperature implied a 15% steeper slope for AuAg@GSH than NaAuAg@GSH advocating sodium-induced thermal stability. We also exposed AuAg@GSH and NaAuAg@GSH under sunlight (99 444 T) and monitored fluorescence intensity at every 45 min interval up to 3 h. Na^+ matrix also contributed photostability preventing photo-oxidation and quenching of fluorescence (for H_2O and O_2).[23] I_t/I_0 (I_0 = fluorescence intensity at exposure time 0 h; I_t = fluorescence intensity at exposure time t h) *vs.* exposure time implied a 39% steeper slope for AuAg@GSH than NaAuAg@GSH advocating sodium-induced photostability [Fig. 3].

2.6 Mechanism of Na^+-induced fluorescence enhancement

FESEM image displayed a similar structure of AuAg@GSH and NaAuAg@GSH. Moreover, EDAX spectra indicated a higher contribution of Ag (along with Na) in comparison to Au, implying that the core–shell structure of AuAg@GSH was not ruptured in NaAuAg@GSH. The solution was stable with a negative zeta potential (−1.09 mV). DLS analysis indicated an average hydrodynamic diameter of 638.8 nm. Particle size distribution was tight with 93% particles at ~605 nm [Fig. 4].

GSH (a thiolated reducing agent) was oxidized to GSSG to reduce Au^{3+} to Au^0 and Ag^+ to Ag^0. Ag^0 was finally converted to Ag_2O (confirmed by various characterization tools) due to aerial oxidation. A positive scaffold stabilized the nanoclusters.[24] The drift of electron density from Au^0_{core} to Ag_2O_{shell} originated synergistic evolution of fluorescent AuAg@GSH clusters.

Wang *et al.*[23] reported the fluorescence enhancement of gold clusters with NaCl due to natural crystallization-induced confinement of the clusters. To simultaneously enhance the luminescence quantum yield and stability of thiolate-protected AuAg@GSH, they were confined into sodium chloride (NaCl) crystals. Mixing AuAg@GSH with a NaCl aqueous solution resulted in a natural crystallization procedure, forming the NaAuAg@GSH crystals. Compared with most other matrix materials, NaCl had the advantages of easy fabrication, low cost, high biosafety, and good transparency. The AuAg@GSH might undergo an adsorption/occlusion coprecipitation through electrostatic interaction[23] with NaCl and be confined into NaCl crystal.

In another mechanism, Na^+ could enhance the positive charge density at the surface, stabilizing AuAg@GSH clusters with improved fluorescence. The zeta potential of NaAuAg@GSH showed that particle surfaces were more positive. Na^+ further assisted the electron travel from core to shell to stabilize AuAg@GSH clusters, causing further fluorescence enhancement (Scheme 2). Thus, Na^+ ions had an intriguing role in brightening AuAg clusters, present in the GSH matrix.[24]

We also varied the counter anions of Na^+. Sodium bicarbonate showed equal enhancement like NaCl. Natural crystallization and protection were available with $NaHCO_3$ and NaCl, unlike NaBr and Na_2CO_3, resulting in Na^+ induced fluorescence enhancement. For the case of NaBr and Na_2CO_3, enhancement was low [Fig. S6, ESI†]. Second mechanism might be ruled out due to the dependence of counter anions on fluorescence enhancement.

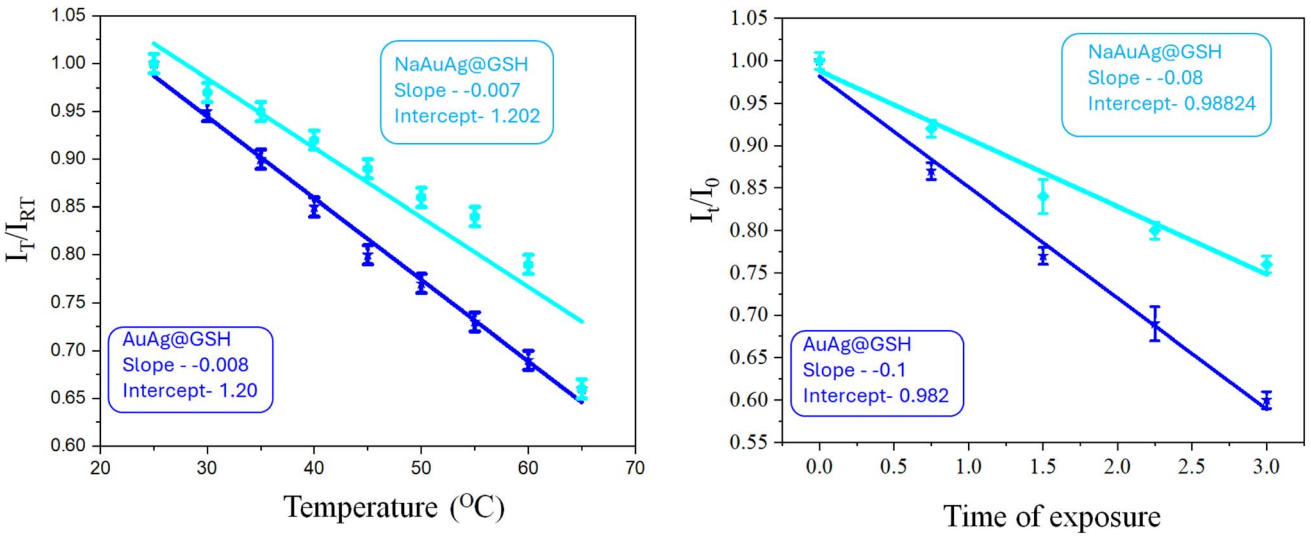

Fig. 3 Alteration of fluorescence of AuAg@GSH and NaAuAg@GSH with temperature variation and sunlight exposure time.

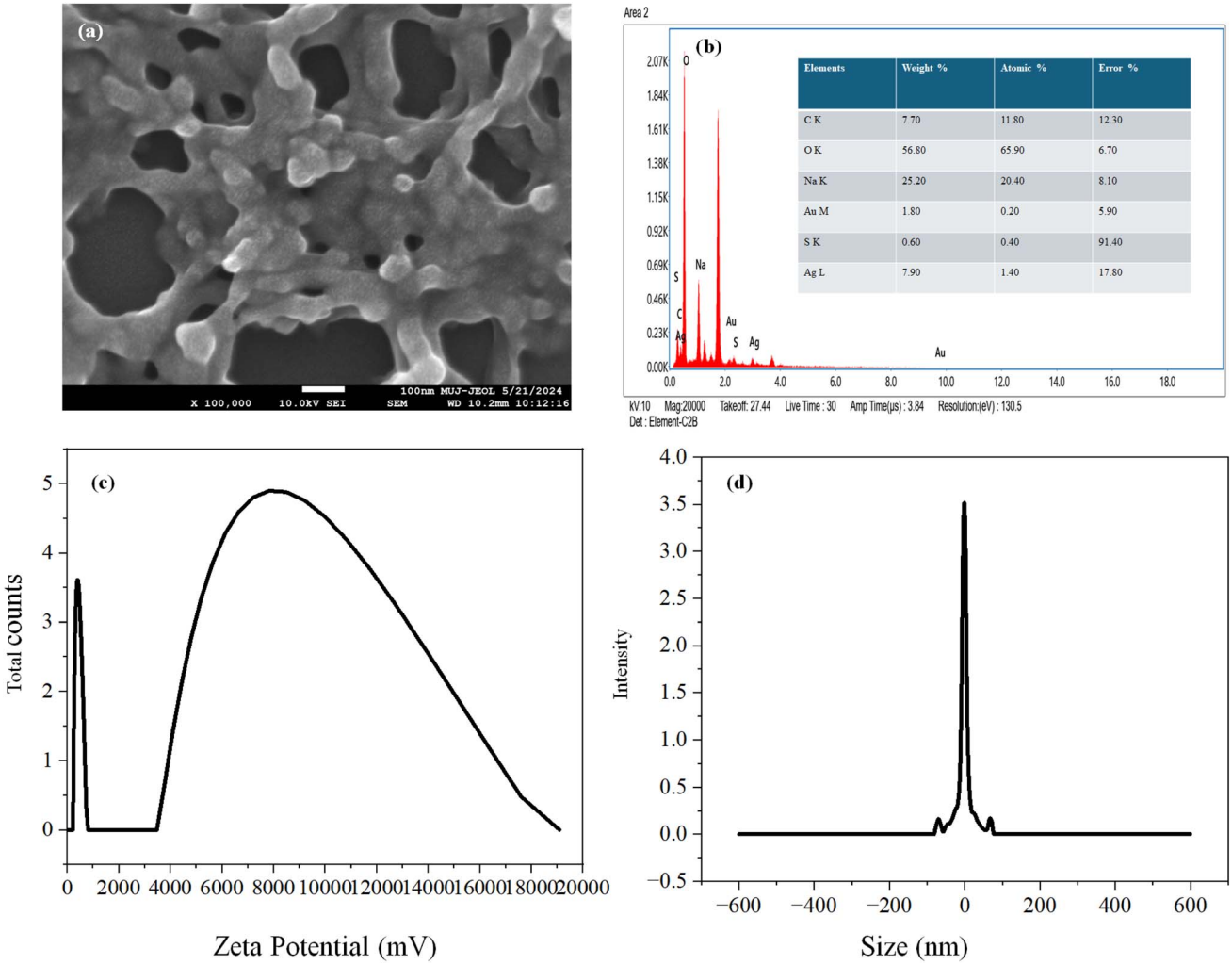

Fig. 4 (a) FESEM, (b) EDAX, (c) zeta potential, and (d) DLS spectra of NaAuAg@GSH.

2.7 Novelty of the work

For the first time, we disclosed Na^+ induced fluorescence enhancement of AuAg bimetallic nanoclusters. Such behaviour helped to sense Na^+ selectively and sensitively. Table 1 summarizes various AuAg nanoclusters. All such clusters had different emission maxima in comparison to our present report.

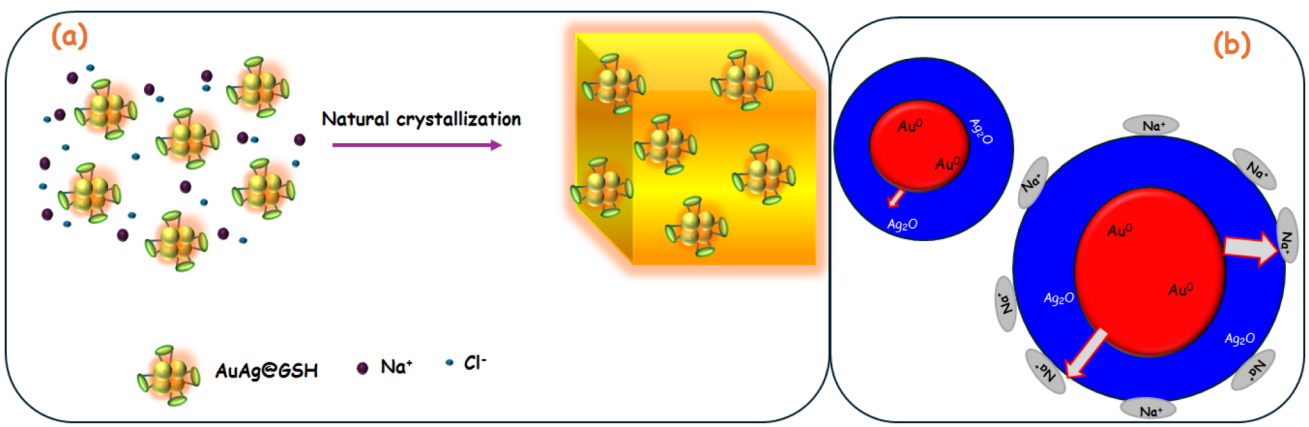

Scheme 2 Mechanism of Na^+ induced fluorescence enhancement based on (a) natural crystallization and confinement, (b) charge redistribution.

Table 4 Various reports of Na^+ sensing using nanoparticles

Sensing platform	Capping agent	λ_{em}	Detection range	Detection limit	Method
Cu–curcumin NPs[25]	Ascorbic acid	530 nm	—	65×10^{-6} M	Colorimetric
Organic NPs[26]	DMSO	350 nm	0 to 25 μM	25 μM	Colorimetric
AuAg@GSH (this work)	GSH	290 nm	10^{-5}–5×10^{-9} M	1.02×10^{-6}	Fluorometric

Na^+ induced brightening of fluorescence was a key novelty of our paper. Table 4 summarizes various sensing platforms for Na^+. There are only a few reports available regarding Na^+ sensing. No one has used fluorometric pathway for Na^+ sensing, before our present report with GSH-protected nanoclusters. We disclosed a unique sensing protocol with plausible mechanisms.

3. Conclusion

Brightening of fluorescence of AuAg nanoclusters, stimulated by Na^+ ions, for the sensing application has been disclosed for the first time in the present paper. Such fluorescence enhancement was quite exclusive, fast and sensitive. Na^+ ion exerted a positive charge matrix for GSH-capped AuAg nanoclusters, exhibiting intriguing fluorescence increment. Basic radial-induced improvement of novel metal clusters (originated synergistically) is expected to be an asset for the young scientist venturing into environmental and medicinal science. Moreover, manipulating the matrix charge to manipulate fluorescence behavior may open a new window for metal ion sensing.

Data availability

The authors are unable or have chosen not to specify which data has been used.

Conflicts of interest

There are no conflicts to declare.

Acknowledgements

We are thankful to CAF (MUJ) and SAIF (MUJ) for instrumental facilities.

Notes and references

1 T. R. Harring, N. S. Deal and D. C. Kuo, Disorders of sodium and water balance, *Emerg. Med. Clin.*, 2014, **32**, 379–401.
2 Z. J. Twardowski, Sodium, hypertension, and an explanation of the "lag phenomenon" in hemodialysis patients, *Hemodial. Int.*, 2008, **12**, 412–425.
3 M. L. M. Firmino, S. Morais, A. N. Correia, P. de Lima-Neto, F. A. O. Carvalho, S. S. L. Castro and T. M. B. F. Oliveira, Sensor based on β-NiOx hybrid film/multi-walled carbon nanotubes composite electrode for groundwater salinization inspection, *Chem. Eng. J.*, 2017, **323**, 47–55.
4 G. R. C. Hamilton, S. K. Sahoo, S. Kamila, N. Singh, N. Kaur, B. W. Hylanda and J. F. Callan, l probes for the detection of protons, and alkali and alkaline earth metal cations, *Chem. Soc. Rev.*, 2015, **44**, 4415–4432.
5 Y. Du, H. Sheng, D. Astruc and M. Zhu, Atomically Precise Noble Metal Nanoclusters as Efficient Catalysts: A Bridge between Structure and Properties, *Chem. Rev.*, 2020, **2**, 526–622.
6 X. Liu, F. Peng, G. Li and K. Diao, Dynamic Metal Nanoclusters: A Review on Accurate Crystal Structures, *Molecules*, 2023, **14**, 5306.
7 M. Yang, L. Zhu, W. Yang and W. Xu, Nucleic acid-templated silver nanoclusters: A review of structures, properties, and biosensing applications, *Coord. Chem. Rev.*, 2023, **491**, 215247.
8 (*a*) Z. Yang, X. Yang, Y. Guao and H. Kawasaki, A Review on Gold Nanoclusters for Cancer Phototherapy, *ACS Appl. Bio Mater.*, 2023, **6**, 4504–4517; (*b*) M. Ganguly, J. Jana, A. Pal and T. Pal, Synergism of gold and silver invites enhanced fluorescence for practical applications, *RSC Adv.*, 2016, **6**, 17683–17703.
9 (*a*) L. Cao, M. Zhou, J. Wang, Q. Zhu, T. Liu, S. Ding and D.-Y. Fu, Gold–Silver Bimetallic Nanoclusters Protected by Glutathione S-Transferase for Colorimetric Sensing of Oxytetracycline, *ACS Appl. Nano Mater.*, 2022, **5**, 11176–11184; (*b*) J. Zhang, Y. Yuan, Y. Wang, F. Sun, G. Laing, Z. Jiang and S. Yu, Microwave-assisted synthesis of photoluminescent glutathione-capped Au/Ag nanoclusters: A unique sensor-on-a-nanoparticle for metal ions, anions, and small molecules, *Environmental*, 2015, **8**, 2329–2339; (*c*) M. Liu, N. Li, Y. He, Y. Ge and G. Song, Dually emitting gold-silver nanoclusters as viable ratiometric fluorescent probes for cysteine and arginine, *Microchim. Acta*, 2018, **185**, 147; (*d*) T.-Y. Zhou, L.-P. Lin, M.-C. Rong, Y.-Q. Jiang and X. Chen, Silver–gold alloy nanoclusters as a fluorescence-enhanced probe for aluminum ion sensing, *Anal. Chem.*, 2013, **20**, 9839–9844; (*e*) M. Ganguly, J. Pal, S. Das, C. Mondal, A. Pal, Y. Negishi and T. Pal, Green synthesis and reversible dispersion of a giant fluorescent cluster in solid and liquid phase, *Langmuir*, 2013, **29**(34), 10945–10958.
10 F. Y. Alzoubi, A. A. Ahmad, I. A. Aljarrah, A. B. Migdadi and Q. M. Al-Bataineh, Localize surface plasmon resonance of silver nanoparticles using Mie theory, *J. Mater. Sci.: Mater. Electron.*, 2023, **34**, 2128.
11 (*a*) R. Jin, Atomically precise metal nanoclusters: stable sizes and optical properties, *Nanoscale*, 2015, **7**, 1549–1565; (*b*) M. Ganguly, C. Mondal, J. Pal and A. Pal, Fluorescent Au(i)@Ag_2/Ag_3 giant cluster for selective sensing of mercury(ii)

ion, *Dalton Trans.*, 2014, **30**, 11557–11565; (*c*) Y. Sun and Y. Xia, Shape-controlled synthesis of gold and silver nanoparticles, *Science*, 2002, **298**, 2176–2179.

12 Z. Bao, Z. Sun, M. Xiao, H. Chen, L. Tian and J. Wang, Transverse oxidation of gold nanorods assisted by selective end capping of silver oxide, *J. Mater. Chem.*, 2011, **21**, 11537–11543.

13 (*a*) P. Kumari and P. Majewski, Adsorption of Albumin on Silica Surfaces Modified by Silver and Copper Nanoparticles, *Nanomaterial*, 2013, **2013**, 1–7; (*b*) I. Maack, M. Osmić, L. Mohrhusen, P. Buhani and K. Al-Shamery, Fitting A Square Peg into A Round Hole: Shape Control in Phase Transfer of Cubic Gold Nanoparticles, *ChemNanoMat*, 2021, **7**, 1–15; (*c*) C. M. Maguire, M. Rosslein, P. Wick and A. Prina-Mello, Characterisation of particles in solution – a perspective on light scattering and comparative technologies, *Sci. Technol. Adv. Mater.*, 2018, **1**, 732–745.

14 P. Attard, Recent advances in the electric double layer in colloid science, *Curr. Opin. Colloid Interface Sci.*, 2001, **6**, 366–371.

15 J. Zhang, Y. Yuan, Y. Wang, F. Sun, G. Liang, Z. Jiang and S.-H. Yu, Microwave-assisted synthesis of photoluminescent glutathione-capped Au/Ag nanoclusters: A unique sensor-on-a-nanoparticle for metal ions, anions, and small molecules, *Nano Res.*, 2015, **8**, 2329–2339.

16 J. Quintana, J. Crespo, A. Falqui, J. M. López-de-Luzuriaga, M. Elena Olmos, M. Rodríguez-Castillo and M. Monge, Mini AuAg Wavy Nanorods Displaying Plasmon-InducedPhotothermal and Photocatalytic Properties, *Adv. Photonics Res.*, 2022, **4**, 2200246.

17 L. Qie, W. Chen, X. Xiong, C. Hu, F. Zou, P. Hu and Y. Huang, Sulfur-Doped Carbon with Enlarged Interlayer Distance as a High-Performance Anode Material for Sodium-Ion Batteries, *Adv. Sci.*, 2015, **2**, 1500195.

18 Z. Wu, M. Wang, J. Yang, X. Zheng, W. Cai, G. Meng, H. Qian, H. Wang and R. Jin, Well-Defi ned Nanoclusters as Fluorescent Nanosensors: A Case Study on Au 25 (SG) 18, *Small*, 2012, **8**, 2028–2035.

19 J. Zhang, Y. Yuan, Y. Wang, F. Sun, G. Liang, Z. Jiang and S.-H. Yu, *Nano Res.*, 2015, **8**, 2329–2339.

20 S.-N. Yin, Y. Liu, C. Zhou and S. Yang, Glutathione-Mediated Cu(I)/Cu(II) Complexes: Valence-Dependent Effects on Clearance and In Vivo Imaging Application, *Nanomaterials*, 2017, **7**, 132.

21 Y.-J. Zhou, Y.-G. Fang, K. Yang, J.-Y. Lin, H.-Q. Li, Z.-J. Chen and Z.-Y. Wang, DBDMH-Promoted Methylthiolation in DMSO: A Metal-Free Protocol to Methyl Sulfur Compounds with Multifunctional Groups, *Molecules*, 2023, **28**, 5635.

22 M. Ganguly, A. Pal, Y. Negishi and T. Pal, Diiminic Schiff Bases: An Intriguing Class of Compounds for a Copper-Nanoparticle-Induced Fluorescence Study, *Chem.–Eur. J.*, 2012, **18**, 15845–15855.

23 M. Wang, B. Duan, Y. Li, S. Jiang, Z. Huang and W. Yang, Glutathione-Capped Au Nanoclusters Embedded in NaCl Crystals for White Light-Emitting Devices, *ACS Appl. Nano Mater.*, 2021, **4**, 7486–7492.

24 (*a*) F. Nuhu, A. Gordon, R. Sturmey, A.-M. Seymour and S. Bhandari, Measurement of Glutathione as a Tool for Oxidative Stress Studies by High Performance Liquid Chromatography, *Molecules*, 2020, **25**, 4196; (*b*) M. Ganguly, C. Mondal, J. Jana, A. Pal and T. Pal, Photoproduced Fluorescent Au(I)@(Ag2/Ag3)-Thiolate Giant Cluster: An Intriguing Sensing Platform for DMSO and Pb(II), *Langmuir*, 2014, **30**(1), 348–357; (*c*) P. Couleaud, S. Adan-Bermudez, A. Aires, S. H Mejías, B. Sot, A. Somoza and A. L. Cortajarena, Designed Modular Proteins as Scaffolds To Stabilize Fluorescent Nanoclusters, *Biomacromolecules*, 2015, **12**, 3836–3844; (*d*) M. Ganguly, A. Pal, Y. Negishi and T. Pal, Synthesis of Highly Fluorescent Silver Clusters on Gold(I) Surface, *Langmuir*, 2013, **29**, 2033–2043.

25 N. Chandran, P. Janardhanan, M. Bayal, R. Pilankatta and S. S Nair, Development of a paper printed colorimetric sensor based on Cu-Curcumin nanoparticles for evolving point-of-care clinical diagnosis of sodium, *Sci. Rep.*, 2022, **15**, 6247.

26 G. Kaur and N. Kaur, Estimation of sodium ions using easily engineered organic nanoparticles-based turn-on fluorescent sensor: Application in biological and environmental samples, *Sens. Actuators*, 2018, **265**, 134–141.